

Inverse-Squeezing Kennedy Receiver for Near-Helstrom Discrimination of Displaced-Squeezed BPSK

Enhao Bai

*Information Support Force Engineering University, Wuhan 430035, China and
Guangxi Key Laboratory of Multimedia Communications and Network Technology, Guangxi University, Nanning 530006, China*

Jian Peng, Tianyi Wu, and Chen Dong^{*}

Information Support Force Engineering University, Wuhan 430035, China

Kai Wen, Fengkai Sun, and Zhenrong Zhang[†]

Guangxi Key Laboratory of Multimedia Communications and Network Technology, Guangxi University, Nanning 530006, China

Chun Zhou

Henan Key Laboratory of Quantum Information and Cryptography, SSF IEU, Zhengzhou 450001, China

Yaping Li

Wuhan Maritime Communication Research Institute, Wuhan 430035, China

(Dated: January 28, 2026)

To address the discrimination problem of binary phase-shift keyed displaced squeezed vacuum states (S-BPSK), this paper proposes an Inverse-squeezing Kennedy (IS-Kennedy) receiver. This architecture incorporates an inverse-squeezing operator following the displacement operation of a conventional Kennedy receiver, mapping the S-BPSK signals onto equivalent large-amplitude coherent states. Furthermore, it employs a photon-number-resolving (PNR) detector to perform maximum a posteriori (MAP) decision-making. Theoretical analysis demonstrates that, under ideal conditions, the IS-Kennedy receiver effectively translates the transmitter's squeezing resources into a displacement gain at the receiver. Consequently, its error probability approaches the Helstrom bound across the entire energy spectrum, remaining within a constant factor of 3 dB. In the low-photon-number regime ($N \approx 0.6$), the proposed scheme surpasses the coherent-state limit, achieving an error rate below 1%. Furthermore, this paper provides an in-depth analysis of system performance under non-ideal conditions, revealing the robustness of PNR detection against background dark counts and a characteristic “parity photon-number step” saturation effect arising from squeezing parameter mismatch.

I. INTRODUCTION

As an important topic in the field of quantum information, quantum-states discrimination directly affects the performance of quantum communication systems. To date, we have consistently regarded coherent states (CSs) as carriers for quantum communication and have proposed numerous excellent discrimination schemes, such as the Kennedy receiver[1], the optimized displacement receiver[2, 3], multi-stage receiver[4–7], the conditional pulse nulling receiver[8], and hybrid receiver [9–12]. This is primarily because coherent states retain their coherence after passing through lossy bosonic channels, demonstrating that they can maintain state purity in most optical transmission media, including but not limited to free space and optical fibers.[13–15]. However, coherent states have inherent discrimination limitations: any two coherent states are non-orthogonal and exhibit overlap in phase space. Since the Helstrom Bound (HB) is closely related to the degree of overlap between quantum states[16, 17], coherent states have a theoretical lower bound on discrimination error probability.

In recent years, quantum-state discrimination schemes based on non-Poissonian photon statistics have attracted widespread attention[18–23]. For example, Giovanni Chesi and Stefano Olivares proposed using squeezed vacuum states ($S(r)|0\rangle$ where $S(r), r \in \mathbf{R}_+$ is squeeze operator and $|0\rangle$ is vacuum state) as information carriers to construct a binary communication channel[21]. By applying a displacement operation $D(\pm\alpha)$ to the squeezed vacuum state, two phase-opposite displaced squeezed vacuum states (DSSs) $|\pm\alpha, r\rangle$ can be generated. Then they encoded BPSK

^{*} dongchengfkd@163.com

[†] zrz76@gxu.edu.cn

symbols into two phase-opposite DSSs (S-BPSK):

$$\begin{cases} \text{symbol '0'} : |\psi_0\rangle = D(-\alpha)S(r)|0\rangle = |-\alpha, r\rangle \\ \text{symbol '1'} : |\psi_1\rangle = D(+\alpha)S(r)|0\rangle = |+\alpha, r\rangle \end{cases} \quad (1)$$

This scheme significantly reduces the overlap between the carrier states by squeezing its position quadrature \hat{X} . Theoretical studies show that when the communication channel energy N is fixed, not only the HB for S-BPSK can be significantly lower than that for BPSK coherent states (C-BPSK), but the error probability of homodyne detection (Standard Quantum Limit, SQL) for S-BPSK can even surpass the HB for C-BPSK at a low mean photon number of $N \approx 0.659$ [21].

Unlike the work of Giovanni Chesi and Stefano Olivares, this paper proposes a quantum-enhanced receiver for discriminating the S-BPSK signal, which is called as the Inverse-squeezing Kennedy Receiver (IS-Kennedy). The IS-Kennedy combines Gaussian operations (displacement and squeeze) and photon-number-resolving detection to approach the Helstrom bound for S-BPSK within a constant factor, while outperforming coherent-state receivers in the low-energy regime. Theoretical analysis shows that, for the same input mean photon number, the IS-Kennedy can achieve an error probability lower than the Helstrom bound for C-BPSK channels in the low-photon-number regime. For example, when $N \approx 0.6$ the error probability falls below 1% in our simulations.

The structure of this paper is as follows: Section II reviews the fundamental theory of S-BPSK discrimination; Section III provides a detailed analysis of the principle and performance of the IS-Kennedy; Section IV explores the performance of IS-Kennedy with an imperfect PNR detector (quantum efficiency η and dark count rate ν); Section V explores the performance of IS-Kennedy under inverse-squeezing parameter mismatch; finally, the paper is summarized, and potential application scenarios are discussed.

II. CHANNEL MODEL AND PERFORMANCE BENCHMARKS

In this section we summarize the signal model and the fundamental performance limits for binary phase-shift keyed (BPSK) communication based on displaced squeezed vacuum states, and we fix the notation used in the rest of the paper.

For binary discrimination between quantum states $|\psi_0\rangle$ and $|\psi_1\rangle$ with prior probabilities $\pi_0 = \pi_1 = \frac{1}{2}$, the minimum error probability (Helstrom bound) is given by [16, 21]:

$$\begin{aligned} P_{\text{HB}}^{\text{DSS}}(\alpha, r) &= \frac{1}{2} \left(1 - \sqrt{1 - |\langle \psi_0 | \psi_1 \rangle|^2} \right) \\ &= \frac{1}{2} \left(1 - \sqrt{1 - \exp(-4\alpha^2 e^{2r})} \right) \end{aligned} \quad (2)$$

As a practically relevant benchmark we also consider homodyne detection along the X quadrature, which attains the standard quantum limit (SQL) for BPSK under ideal conditions. Given the input is $\rho_i = |\psi_i\rangle \langle \psi_i|$, the conditional probability density of the homodyne outcome x ,

$$\begin{aligned} P(x|\rho_i) &= \int_{-\infty}^{+\infty} dp \cdot W(x, p|\rho_i) \\ &= \frac{e^r}{\sqrt{\pi}} \exp \left\{ -e^{2r} \left[x - (-1)^{i+1} \sqrt{2} \alpha \right]^2 \right\}, \quad i \in 0, 1, \end{aligned} \quad (3)$$

which $W(x, p|\rho_i)$ is the Wigner function of ρ_i (see Appendix). And the resulting error probability is

$$P_{\text{SQL}}^{\text{DSS}} = \int_0^{+\infty} P(x|\rho_0) dx = \frac{1}{2} \text{erfc} \left(\sqrt{2} \alpha e^r \right) \quad (4)$$

To parameterize the contribution of squeezing, we introduce the squeezing fraction

$$\beta \triangleq \frac{\sinh^2(r)}{N} \quad (5)$$

which quantifies the share of the total energy ($N = |\alpha|^2 + \sinh^2(r)$) stored in squeezing [21]. Therefore, the parameter α and r can be expressed as

$$\begin{cases} \alpha = \sqrt{N(1-\beta)}, \quad r = \sinh^{-1} \sqrt{N\beta} \\ \alpha e^r = \sqrt{N(1-\beta)} \left(\sqrt{1+N\beta} + \sqrt{N\beta} \right) \end{cases} \quad (6)$$

Accordingly, both the Helstrom bound and the SQL for S-BPSK become functions of (N, β) , denoted $P_{\text{SQL}}^{\text{DSS}}(N, \beta)$, and $P_{\text{HB}}^{\text{DSS}}(N, \beta)$. The squeezing fraction can be optimized at fixed total energy. By minimizing $P_{\text{HB}}^{\text{DSS}}(N, \beta)$ over β one obtains the optimal value [21]:

$$\beta_{\text{opt}}(N) = \frac{N}{2N+1}, \quad \alpha e^r = \sqrt{N(N+1)} \quad (7)$$

Both the Helstrom bound and the SQL for S-BPSK are rewritten as:

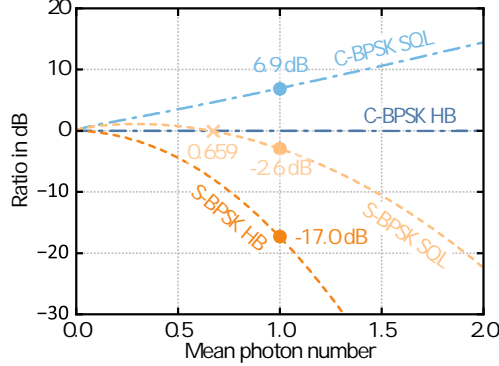


FIG. 1. The ratios of $P_{\text{HB}}^{\text{DSS}}(N, \beta_{\text{opt}})$, $P_{\text{SQL}}^{\text{DSS}}(N, \beta_{\text{opt}})$ and $P_{\text{SQL}}^{\text{CS}}(N)$ to $P_{\text{HB}}^{\text{CS}}(N)$ vs. input state energy N . Here, $P_{\text{SQL}}^{\text{CS}}(N) = \frac{1}{2} \left[1 - \text{erf} \left(\sqrt{2 \cdot N} \right) \right]$ and $P_{\text{HB}}^{\text{CS}}(N) = \frac{1}{2} \left[1 - \sqrt{1 - \exp \{ -4 \cdot N \}} \right]$.

$$P_{\text{SQL}}^{\text{DSS}}(N, \beta_{\text{opt}}) = \frac{1}{2} \text{erfc} \left(\sqrt{2N(N+1)} \right) \quad (8)$$

$$P_{\text{HB}}^{\text{DSS}}(N, \beta_{\text{opt}}) = \frac{1}{2} \left(1 - \sqrt{1 - \exp \{ -4N(N+1) \}} \right) \quad (9)$$

When the DSSs are prepared with this choice, the S-BPSK Helstrom bound is significantly lower than that of C-BPSK at the same energy. In particular, for $N \approx 1$ the S-BPSK Helstrom bound already reaches the order of 10^{-4} , whereas C-BPSK requires approximately twice the energy to achieve a comparable error probability. Moreover, in the low-photon number regime the S-BPSK SQL can fall below the Helstrom bound of C-BPSK, with the crossover occurring around $N \approx 0.659$ (see Fig. 1). At $N = 1.0$, the HB for S-BPSK surpasses the SQL for C-BPSK by a remarkable 17.39dB, and the SQL for S-BPSK also is 2.94dB lower. In the subsequent analyses, all DSSs employ the optimal squeezing fraction β_{opt} .

III. INVERSE-SQUEEZING KENNEDY RECEIVER UNDER IDEAL CONDITIONS

In this section, we propose a novel receiver architecture for S-BPSK discrimination: the Inverse-squeezing Kennedy (IS-Kennedy) receiver. The schematic structure is illustrated in Fig. 2. Compared to the conventional Kennedy receiver, the IS-Kennedy incorporates two key modifications: (i) the insertion of an inverse-squeezing (IS) module after the displacement operation, which applies the operator $S(-r)$ to the signal; and (ii) the upgrade of the terminal single-photon detector (SPD) to a photon-number-resolving detector (PNRD), enabling maximum a posteriori (MAP) decision-making under generalized statistical models. The squeezing amplitude of the IS module is matched to that of the transmitter, while the squeezing axis is rotated by $\pi/2$ (orthogonal) relative to the transmitter. This configuration cancels the initial squeezing and produces an equivalent amplification of the signal's mean photon number. Effectively, the IS-Kennedy converts the transmitter's squeezing resources into an equivalent amplitude gain at the receiver, thereby reducing the S-BPSK discrimination problem to an ‘‘amplified Kennedy nulling problem.’’ Furthermore, the PNRD provides the necessary statistical degrees of freedom for optimal MAP decisions under non-ideal conditions, which will be discussed later.

Let the input S-BPSK signal be denoted as $\rho_i \sim |\psi_i\rangle$, where $|\psi_i\rangle = D(\pm\alpha)S(r)|0\rangle$. First, the input signal interferes with a local oscillator (LO) on a highly transmissive beam splitter ($\tau \rightarrow 1$) to perform the Kennedy nulling displacement. Consequently, the S-BPSK alphabet is mapped to a squeezed OOK (S-OOK) alphabet σ_i :

$$\sigma_i \sim D(\alpha)|\psi_i\rangle = \begin{cases} S(r)|0\rangle, & i = 0, \\ D(2\alpha)S(r)|0\rangle, & i = 1. \end{cases} \quad (10)$$

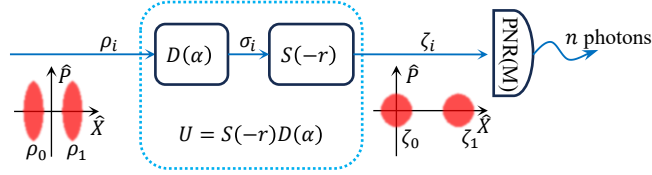


FIG. 2. Schematic of the proposed Inverse-squeezing Kennedy (IS-Kennedy) receiver. The input state ρ_i is first processed by a Kennedy-type nulling displacement $D(\alpha)$, which maps the BPSK displaced squeezed states (S-BPSK) to a squeezed OOK pair (S-OOK). A subsequent inverse-squeezing operation $S(-r)$ converts the two hypotheses from the displaced squeezed alphabet into an amplified coherent-state alphabet (C-OOK), ideally $\{|0\rangle, |2\alpha e^r\rangle\}$ in the matched case. The resulting state ζ_i is measured by a photon-number-resolving (PNR) detector yielding outcome n , and the final decision is made according to the maximum a posteriori (MAP) criterion.

Subsequently, σ_i passes through the IS module, mapping the S-OOK alphabet to a coherent-state OOK (C-OOK) alphabet ζ_i :

$$\zeta_i = S(-r)\sigma_i S^\dagger(-r) \sim \begin{cases} S(-r)S(r)|0\rangle = |0\rangle, & i = 0, \\ S(-r)D(2\alpha)S(r)|0\rangle = D(2\alpha e^r)|0\rangle = |2\gamma\rangle, & i = 1. \end{cases} \quad (11)$$

In the general case, $\gamma = \alpha \cosh r + \alpha^* \sinh r$. Under the condition $\alpha \in \mathbb{R}_+$ adopted in this work, $\gamma = \alpha e^r$. Therefore, we define:

$$\gamma \triangleq \alpha e^r, \quad N_{\text{eff}} \triangleq |\gamma|^2 = |\alpha|^2 e^{2r}. \quad (12)$$

With the optimal energy allocation β_{opt} , the effective photon number can be further expressed as $N_{\text{eff}} = N(N+1) > N$. This indicates that the IS module transforms the transmitter's squeezing resources into a “coherent-state separation gain” directly accessible by the receiver. This results in a larger Euclidean distance between the two states in phase space (Fig. 3(a-c)) and simultaneously reduces the overlap of the Fock-basis populations of ζ_i (Fig. 3(e-f)).

Next, PNR detection is performed on ζ_i , yielding an output photon number n . The positive operator-valued measure (POVM) for an ideal PNR detector is given by:

$$\Pi_n^{\text{ideal}} = |n\rangle\langle n|, \quad n = 0, 1, 2, \dots \quad (13)$$

From Eq. (11), we have $\zeta_0 = |0\rangle\langle 0|$ and $\zeta_1 = |2\gamma\rangle\langle 2\gamma|$, with mean photon numbers $\mu_0 = 0$ and $\mu_1 = |2\gamma|^2 = 4N_{\text{eff}}$, respectively. Thus, the probability of detecting n photons given transmitted symbol i is:

$$P(n|i) = \text{Tr}(\zeta_i \Pi_n^{\text{ideal}}) = \begin{cases} \text{Poiss}(n; \mu_0) = \delta_{0,n}, & i = 0, \\ \text{Poiss}(n; \mu_1), & i = 1, \end{cases} \quad (14)$$

where $\text{Poiss}(n; \mu) = e^{-\mu} \frac{\mu^n}{n!}$. The posterior probabilities are given by:

$$P(i=0|n) = \frac{\pi_0 P(n|i=0)}{\sum_k \pi_k P(n|i=k)}, \quad P(i=1|n) = \frac{\pi_1 P(n|i=1)}{\sum_k \pi_k P(n|i=k)}. \quad (15)$$

The MAP decision rule is defined as:

$$\hat{i}(n) = \begin{cases} 1, & P(i=1|n) \geq P(i=0|n), \\ 0, & \text{otherwise.} \end{cases} \quad (16)$$

Assuming equal priors ($\pi_0 = \pi_1 = 1/2$), the log-likelihood ratio is:

$$L(n) = \ln \frac{P(n|i=0)}{P(n|i=1)} = \ln \frac{\text{Poiss}(n; \mu_0)}{\text{Poiss}(n; \mu_1)} = -\mu_0 + \mu_1 + n \ln \left(\frac{\mu_0}{\mu_1} \right). \quad (17)$$

Since $L(n)$ is a monotonic function of n , the MAP decision (Eq. (16)) is equivalent to a threshold detection:

$$\hat{i}(n) = \begin{cases} 1, & n \geq n_{\text{th}}, \\ 0, & \text{otherwise.} \end{cases} \quad (18)$$

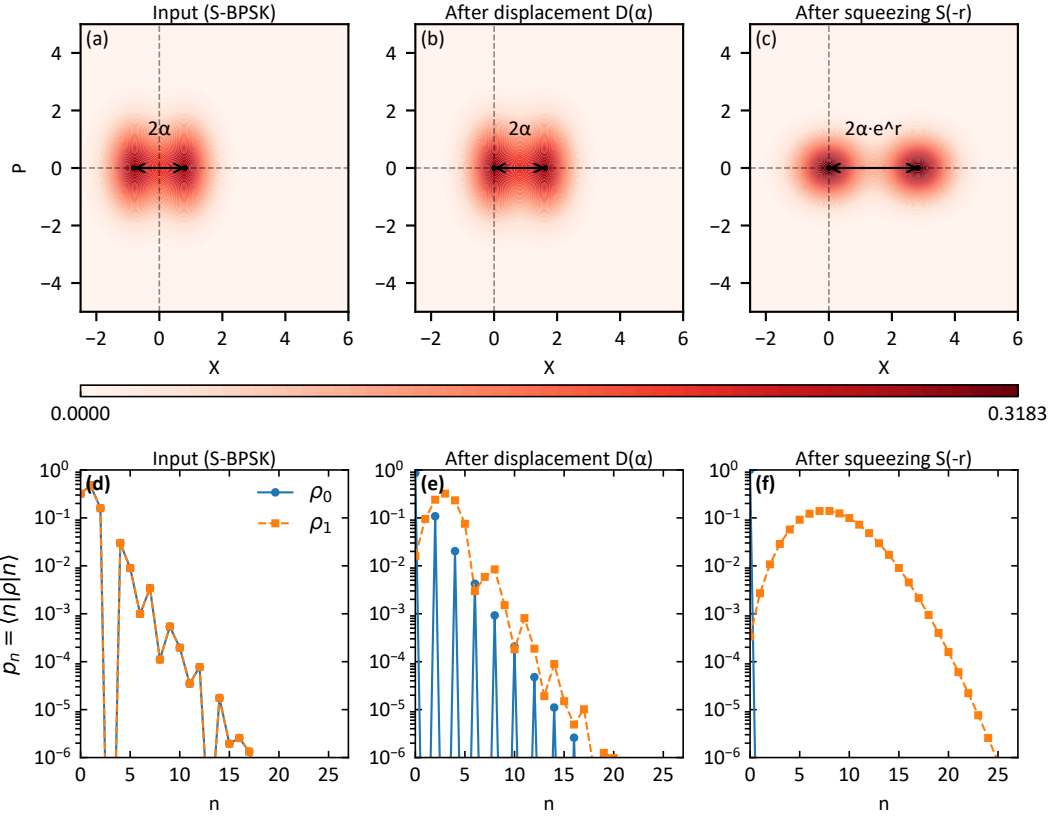


FIG. 3. Phase-space representations (a–c) and Fock-basis populations (d–f) of the input states ρ_i in the IS-Kennedy for mean photon number $N = 1.0$ and squeezing fraction $\beta = \beta_{\text{opt}}$. Panels (a) and (d) show the input states ρ_i ; panels (b) and (e) show the states after the full IS-Kennedy transformation $\sigma_i = D(\alpha)\rho_i D^\dagger(\alpha)$. Panels (c) and (f) show the states after inverse-squeezing (IS) $\zeta_i = U\rho_i U^\dagger$ with $U = S(-r)D(\alpha)$.

The optimal threshold n_{th}^* corresponds to the zero-crossing of the log-likelihood ratio:

$$n_{\text{th}}^* = \left\lceil \frac{\mu_1 - \mu_0}{\ln \mu_1 - \ln \mu_0} \right\rceil. \quad (19)$$

Under ideal conditions where $\mu_0 = 0$, we have $\lim_{\mu_0 \rightarrow 0} \frac{\mu_1 - \mu_0}{\ln \mu_1 - \ln \mu_0} \rightarrow 0^+$; thus, $n_{\text{th}}^* = 1$. This corresponds to a standard on-off detection strategy, implying that a simple single-photon detector (SPD) suffices to achieve PNR performance in this ideal limit. It is important to emphasize, however, that the introduction of the PNRD is not intended to improve the limit of “ideal nulling with matched squeezing.” Rather, it addresses practical system imperfections: once squeezing mismatch or detector imperfections (efficiency/dark counts) occur, ζ_0 deviates from the vacuum state, yielding a non-zero $P(n \geq 1 | i = 0)$. In such cases, the optimal decision is no longer a simple on-off rule, and the PNRD provides the necessary statistical information to implement a generalized MAP or optimal threshold strategy. Quantitative analysis of these non-ideal factors is presented in subsequent sections.

The false alarm probability P_{FA} (deciding 1 when 0 is sent) and the miss detection probability P_{Mi} (deciding 0 when 1 is sent) are:

$$P_{\text{FA}} = P(n \geq n_{\text{th}}^* | i = 0), \quad P_{\text{Mi}} = P(n < n_{\text{th}}^* | i = 1). \quad (20)$$

Therefore, under equal priors and ideal conditions ($n_{\text{th}}^* = 1$), the average error probability of the IS-Kennedy is:

$$\begin{aligned} P_{\text{err}}^{\text{IS-K,ideal}} &= \frac{1}{2} (P_{\text{FA}} + P_{\text{Mi}}) \\ &= \frac{1}{2} [1 - P(n = 0 | i = 0) + P(n = 0 | i = 1)] \\ &= \frac{1}{2} \exp(-|2\gamma|^2) = \frac{1}{2} \exp(-4N_{\text{eff}}). \end{aligned} \quad (21)$$

Substituting the optimal energy allocation condition $N_{\text{eff}} = N(N + 1)$, we obtain:

$$P_{\text{err}}^{\text{IS-K,ideal}} = \frac{1}{2} \exp[-4N(N + 1)]. \quad (22)$$

Notably, we observe that:

$$P_{\text{err}}^{\text{IS-K,ideal}}(N) = P_{\text{err}}^{\text{K,ideal}}(N_{\text{eff}}), \quad (23)$$

where $P_{\text{err}}^{\text{K,ideal}}$ is the error probability of the conventional Kennedy receiver under ideal conditions [1]. This implies that, under matched squeezing, the IS-Kennedy is equivalent to mapping an S-BPSK signal with mean photon number N to a C-BPSK signal with mean photon number N_{eff} via the IS module, followed by Kennedy nulling and on-off detection.

For S-BPSK, the Helstrom bound in Eq. (9) and the IS-Kennedy error probability in Eq. (22) satisfy the relation:

$$\frac{P_{\text{err}}^{\text{IS-K,ideal}}}{P_{\text{HB}}^{\text{DSS}}} = \frac{\exp\{-4N(N + 1)\}}{1 - \sqrt{1 - \exp\{-4N(N + 1)\}}}. \quad (24)$$

In the low-energy limit $N \rightarrow 0$, both $P_{\text{err}}^{\text{IS-K}}$ and $P_{\text{HB}}^{\text{DSS}}$ approach 0.5, and their ratio approaches 1, corresponding to random guessing. In the high-energy regime $N \gg 1$, the ratio approaches 2 (i.e., 3 dB), yielding:

$$P_{\text{err}}^{\text{IS-K,ideal}} \simeq 2P_{\text{HB}}^{\text{DSS}}. \quad (25)$$

Although the IS-Kennedy remains suboptimal with respect to the S-BPSK Helstrom bound, satisfying $P_{\text{err}}^{\text{IS-K}} \in [P_{\text{HB}}^{\text{DSS}}, 2P_{\text{HB}}^{\text{DSS}}]$ for all N , it provides a substantial advantage over C-BPSK channels. Specifically, for the same mean photon number N , the proposed IS-Kennedy achieves an error probability strictly lower than the Helstrom bound $P_{\text{HB}}^{\text{CS}}$ of a C-BPSK channel. For instance, around $N \approx 0.4$ in Fig. 4, the IS-Kennedy performance lies between the DSS Helstrom bound and the coherent-state Helstrom bound.

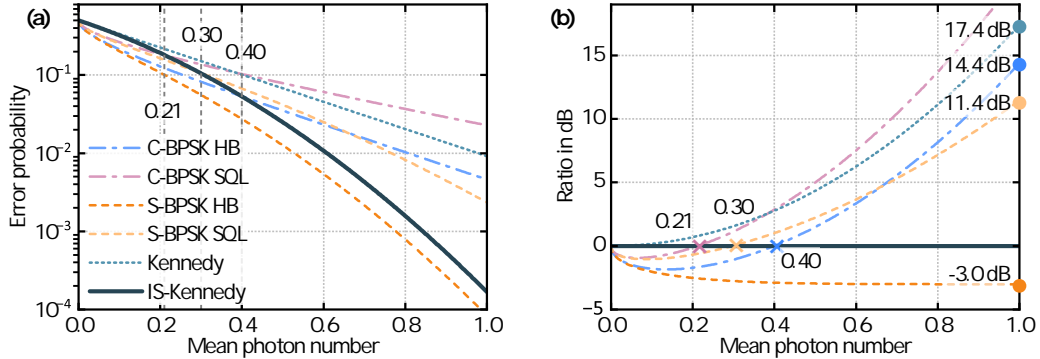


FIG. 4. Performance of the IS-Kennedy under ideal conditions. (a) Error probability of the IS-Kennedy. (b) Ratio (in dB) of the benchmarks $P_{\text{HB}}^{\text{CS}}$, $P_{\text{SQL}}^{\text{CS}}$, $P_{\text{HB}}^{\text{DSS}}$, $P_{\text{SQL}}^{\text{DSS}}$, and $P_{\text{err}}^{\text{K,ideal}}$ relative to $P_{\text{err}}^{\text{IS-K,ideal}}$.

Figure 4(a) shows the IS-Kennedy error probability as a function of the mean photon number N under ideal conditions, alongside the Kennedy receiver and benchmarks for C-BPSK and S-BPSK discrimination. The IS-Kennedy surpasses the C-BPSK SQL, the S-BPSK SQL, and the C-BPSK Helstrom bound at approximately $N \approx 0.21, 0.30$, and 0.40 , respectively. The performance advantage over these benchmarks increases with N , consistent with the fact that $P_{\text{err}}^{\text{IS-K}} = \frac{1}{2} \exp[-4N(N + 1)]$ features an approximately quadratic exponent $N(N + 1)$, leading to a steeper decay than the linear scaling of coherent-state benchmarks. The dB ratios summarized in Fig. 4(b) quantify these advantages. At $N = 1.0$, the IS-Kennedy achieves gains of 21.3 dB, 11.4 dB, and 14.4 dB relative to the C-BPSK SQL, the S-BPSK SQL, and the C-BPSK Helstrom bound, respectively. Additionally, the IS-Kennedy significantly outperforms the conventional Kennedy receiver, exhibiting a 17.4 dB gain at $N = 1.0$. Meanwhile, it remains 3 dB above the S-BPSK Helstrom bound, staying within a constant factor of the ultimate quantum limit. These results demonstrate that the IS-Kennedy delivers robust performance over a broad photon-number regime under ideal conditions.

IV. IS-KENNEDY RECEIVER WITH AN IMPERFECT PNR DETECTOR

The previous section presented the closed-form error probability of the IS-Kennedy receiver under ideal detection conditions, pointing out that with perfect nulling and matched squeezing, the optimal decision rule degenerates to

a simple on-off strategy. However, in practical implementations, PNR detectors possess finite resolution (maximum resolvable photon number, M) and suffer from non-ideal factors such as limited detection efficiency and dark counts (background counts). In this section, while maintaining the assumption of an ideal IS-Kennedy processing module (i.e., retaining $\zeta_0 = |0\rangle\langle 0|$ and $\zeta_1 = |2\gamma\rangle\langle 2\gamma|$), we analyze the impact of imperfect PNR detection on the error probability and derive the expression for the optimal threshold (MAP-equivalent) decision and the corresponding error probability.

Considering an imperfect detection efficiency $\eta \in (0, 1]$ and a mean dark count rate $\nu \geq 0$, the POVM operators are described by [24, 25]:

$$\Pi_n^{(\eta, \nu)} = e^{-\nu} \sum_{l=0}^n \sum_{k=n-l}^{\infty} \frac{\nu^l}{l!} \binom{k}{n-l} \eta^{n-l} (1-\eta)^{k-(n-l)} |k\rangle\langle k|. \quad (26)$$

Consequently, the probability of detecting n photons (Eq. (14)) is reformulated as:

$$P(n|i) = \text{Tr} \left\{ \zeta_i \Pi_n^{(\eta, \nu)} \right\} = \begin{cases} \text{Poiss}(n; \eta\mu_0 + \nu), & i = 0, \\ \text{Poiss}(n; \eta\mu_1 + \nu), & i = 1, \end{cases} \quad (27)$$

where $\mu_0 = 0$ and $\mu_1 = |2\gamma|^2 = 4N_{\text{eff}}$. The log-likelihood ratio (Eq. (17)) is updated to:

$$L(n) = -\eta\mu_0 + \eta\mu_1 + n \ln \frac{\eta\mu_0 + \nu}{\eta\mu_1 + \nu}, \quad (28)$$

which remains a monotonic function of n . Therefore, the MAP criterion is equivalent to a threshold detection scheme. Taking the PNR detector's resolution M into account (denoted as PNR(M)), the optimal threshold (Eq. (19)) involves a truncation at M :

$$n_{\text{th}}^* = \min \left\{ \left\lceil \frac{\eta\mu_1 - \eta\mu_0}{\ln(\eta\mu_1 + \nu) - \ln(\eta\mu_0 + \nu)} \right\rceil, M \right\} = \min \left\{ \left\lceil \frac{4\eta N_{\text{eff}}}{\ln(4\eta N_{\text{eff}} + \nu) - \ln \nu} \right\rceil, M \right\}. \quad (29)$$

From the above equation, the adaptive behavior of the IS-Kennedy receiver against different non-ideal factors can be observed:

- **Presence of dark counts ($\nu > 0$):** The denominator decreases, resulting in an optimal threshold $n_{\text{th}}^* > 1$. This implies that the PNR detector can filter out background noise by raising the decision threshold, demonstrating its robustness advantage over a standard single-photon detector (SPD).
- **Negligible dark counts ($\nu \rightarrow 0$):** The denominator approaches infinity, leading to $n_{\text{th}}^* \rightarrow 1$. In this limit, the optimal strategy reverts to the standard on-off decision. This indicates that in a pure loss channel ($\eta < 1, \nu = 0$), the PNR detector offers no performance gain over an SPD, as simple presence/absence detection is optimal.

Figure 5 illustrates the performance of the IS-Kennedy receiver with imperfect detectors. As shown in Fig. 5(b) and (d), the error probability and the gain relative to the SQL exhibit a characteristic oscillatory or “step-like” behavior when dark counts are significant. This phenomenon is intrinsic to the discreteness of PNR detection. As the signal energy N increases, the optimal likelihood ratio varies continuously, whereas the physical decision threshold n_{th}^* must remain an integer. Consequently, n_{th}^* stays constant over intervals of N (see Fig. 5(c)) before discretely jumping to the next integer level. These jumps allow the receiver to adaptively filter out higher dark-count rates, maintaining robust performance even when ν is large (e.g., $\nu = 10^{-2}$).

Notably, Fig. 5(a) reveals that while the detection efficiency η impacts the rate of error decay (the slope), the saturation error floor at high energies is dictated solely by the dark count rate ν . In the high-energy regime ($N \gg 1$), the miss detection probability (Eq. (20)) rapidly approaches zero. Consequently, the error probability (saturation floor) is dominated by the false alarm probability, with the optimal threshold saturating at $n_{\text{th}}^* = M$:

$$P_{\text{sat}} \approx \frac{1}{2} P_{\text{FA}} = \frac{1}{2} e^{-\nu} \sum_{n=M}^{+\infty} \frac{\nu^n}{n!} \xrightarrow{\text{Taylor series}} \frac{1}{2} (1 - \nu + \dots) \sum_{n=M}^{+\infty} \frac{\nu^n}{n!}. \quad (30)$$

Given that the dark count rate of practical PNR detectors is typically much less than unity ($\nu \ll 1$) [26], the dominant contribution to the summation comes from the first term, $n = M$. Thus, the saturation error probability can be approximated as:

$$P_{\text{sat}} \approx \frac{1}{2} \frac{\nu^M}{M!}. \quad (31)$$

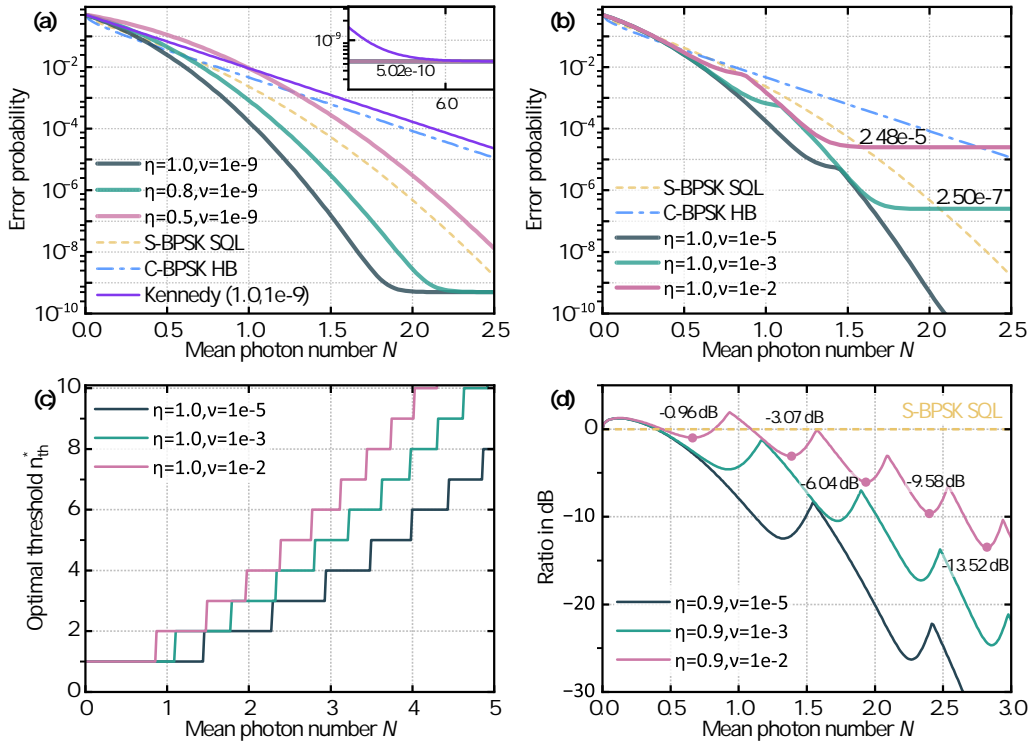


FIG. 5. Performance analysis of the IS-Kennedy receiver under imperfect detection conditions. (a) Error probability of IS-Kennedy with SPD for varying detection efficiencies $\eta \in \{1.0, 0.8, 0.5\}$ and extremely small dark counts ($\nu = 10^{-9}$). (b) Error probability of IS-Kennedy with PNR(2) under different dark count rates ν (with $\eta = 1.0$). The “step-like” behavior in the error curves arises from the discrete nature of the optimal decision threshold. (c) The optimal detection threshold n_{th}^* as a function of signal energy for different dark count rates, calculated via Eq. (29). The jumps in threshold correspond exactly to the inflection points observed in panels (b) and (d). (d) The performance ratio (in dB) of the IS-Kennedy with PNR(10) relative to the S-BPSK SQL. The oscillatory behavior reflects the discrete adjustment of n_{th}^* to balance signal detection against dark count noise.

This expression indicates that the saturation error probability of the IS-Kennedy receiver is independent of detection efficiency η and mean photon number N , depending instead on the PNR detector’s resolution M and dark count rate ν . Therefore, the existence of any non-zero dark count, however small, inevitably leads to an error probability saturation. Furthermore, in conjunction with Eq. (23), since the advantage of the IS-Kennedy equipped with an SPD lies in converting squeezing resources into effective energy gain rather than suppressing noise floor, its saturation error probability is identical to that of the conventional Kennedy receiver (see Fig. 5(a)).

V. IS-KENNEDY RECEIVER WITH SQUEEZING MISMATCH

In the preceding sections, we assumed that the IS module at the receiver could perfectly execute the $S(-r)$ operation, thereby precisely converting the squeezing resources into an enhanced energy gain. However, in practical experimental setups, deviations between the receiver’s squeezing parameters and the input signal are inevitable due to factors such as optical loss, pump fluctuation, and phase locking errors. This phenomenon is referred to as squeezing mismatch (SM).

Without loss of generality, we adopt a simplified model where the transmitter performs perfect squeezing and the optical path is lossless, attributing all squeezing adaptation errors solely to the IS module. Let the squeezing parameter applied by the IS module be denoted as:

$$z_s = (-r + \Delta r) e^{j\Delta\theta}, \quad j = \sqrt{-1}, \quad (32)$$

where Δr represents the magnitude mismatch and $\Delta\theta$ represents the phase mismatch. Under ideal conditions, $\Delta r = \Delta\theta = 0$.

Let the input S-BPSK signal be $\rho_i \sim |\psi_i\rangle$, with $|\psi_i\rangle = D(\pm\alpha)S(r)|0\rangle$. Under mismatch conditions, the overall transformation of the receiver is given by:

$$\zeta_i \sim S(z_s)D(\alpha)|\psi_i\rangle = \begin{cases} S_{\text{tot}}|0\rangle, & i = 0, \\ S_{\text{tot}}|2\gamma\rangle, & i = 1. \end{cases} \quad (33)$$

Here, the composite squeezing operator is defined as $S_{\text{tot}} \triangleq S(z_s)S(r)$, which reduces to the identity operator $S_{\text{tot}} = \mathbb{I}$ in the ideal case. Thus, the essence of the mismatch is encapsulated within S_{tot} . Using the single-mode Gaussian operator decomposition, this operator can always be expressed as:

$$S_{\text{tot}} = R(\vartheta)S(z_m), \quad (34)$$

where $R(\vartheta) = \exp(-j\vartheta a^\dagger a)$ is a phase rotation, and $S(z_m)$ represents the equivalent residual squeezing with parameter $z_m = r_m e^{j\theta_m}$. Since $R(\vartheta)$ contributes only a phase factor in the Fock basis and does not alter the photon number distribution, the impact of mismatch on PNR statistics for a given energy N is determined solely by the residual squeezing parameters (r_m, θ_m) .

Next, we determine (r_m, θ_m) using the Bogoliubov transformation. Letting $r_s \triangleq -r + \Delta r$ and $\theta_s \triangleq \Delta\theta$, the coefficients for the transformation $S_{\text{tot}}^\dagger a S_{\text{tot}} = xa + ya^\dagger$ are derived as:

$$x = \cosh(r_s) \cosh r + e^{j\theta_s} \sinh(r_s) \sinh r, \quad y = -\cosh(r_s) \sinh r - e^{j\theta_s} \sinh(r_s) \cosh r, \quad (35)$$

satisfying the unitarity condition $|x|^2 - |y|^2 = 1$. Consequently, we obtain:

$$r_m = \text{arcsinh}(|y|), \quad \vartheta = -\arg(x), \quad \theta_m = \arg(-y) - \arg(x). \quad (36)$$

In practical scenarios characterized by small mismatches ($\Delta r \ll 1$, $|\Delta\theta| \ll 1$) [27, 28], a first-order approximation yields:

$$y \approx -\Delta r + j \frac{\Delta\theta}{2} \sinh(2r), \quad (37)$$

which leads to:

$$\begin{aligned} r_m &\approx \sqrt{(\Delta r)^2 + \left(\frac{\Delta\theta}{2} \sinh 2r\right)^2}, \\ \theta_m &\approx \arg\left(\Delta r - j \frac{\Delta\theta}{2} \sinh(2r)\right) + \Delta\theta \sinh^2 r. \end{aligned} \quad (38)$$

It is worth highlighting the asymmetric sensitivity revealed by Eq. (38): the total residual squeezing r_m is significantly more sensitive to the phase mismatch $\Delta\theta$ than to the magnitude mismatch Δr . This arises because the phase mismatch term is scaled by the coefficient $\frac{1}{2} \sinh(2r)$, which grows rapidly with the squeezing parameter r (and thus the signal energy N). This leads to a “dominant masking effect”: in the presence of non-negligible phase mismatch, its contribution to r_m typically far exceeds that of the magnitude mismatch. Given the geometric relationship $r_m \approx \sqrt{(\Delta r)^2 + (K\Delta\theta)^2}$, the value of r_m becomes almost entirely determined by the phase mismatch term. This explains the phenomenon observed in the simulation results (see Fig. 6(a) and (b)), where the error probability curves for $(\Delta r, \Delta\theta) = (0.00, 0.03\pi)$ and $(0.02, 0.03\pi)$ nearly coincide. Consequently, in experimental systems, the requirement for phase locking precision is much more stringent than that for amplitude matching.

Phase-only mismatch ($\Delta r = 0$):

$$\begin{aligned} r_m &\approx \frac{|\Delta\theta|}{2} \sinh(2r) = |\Delta\theta| \frac{N(N+1)}{2N+1}, \\ \theta_m &\approx -\frac{\pi}{2} \text{sgn}(\Delta\theta) + \Delta\theta \sinh^2 r = -\frac{\pi}{2} \text{sgn}(\Delta\theta) + \Delta\theta \frac{N^2}{2N+1}, \quad (\text{mod } 2\pi). \end{aligned} \quad (39)$$

Amplitude-only mismatch ($\Delta\theta = 0$):

$$r_m \approx |\Delta r|, \quad \theta_m \approx \begin{cases} 0, & \Delta r > 0, \\ \pi, & \Delta r < 0, \end{cases} \quad (\text{mod } 2\pi). \quad (40)$$

We now calculate the photon number probability distribution of ζ_i . Ignoring the rotation $R(\vartheta)$ which does not affect photon statistics, the equivalent output states derived from Eq. (34) are:

$$\zeta_0 \sim S(z_m) |0\rangle, \quad \zeta_1 \sim S(z_m) |2\gamma\rangle. \quad (41)$$

To utilize standard photon number distribution formulas, we rewrite $|\zeta_1\rangle$ as a displaced squeezed vacuum state:

$$S(z_m) |2\gamma\rangle = D(2\gamma_m) S(z_m) |0\rangle, \quad (42)$$

where

$$\gamma_m = \gamma \cosh r_m + \gamma^* e^{i\theta_m} \sinh r_m. \quad (43)$$

Consequently, the Poissonian distribution valid for the ideal IS-Kennedy (Eq. (14)) no longer applies. For an ideal PNR(M) detector (considering only finite resolution), the probability of detecting n photons given symbol i is:

$$P(n|i) = \text{Tr}(\Pi_n \zeta_i) = \begin{cases} p_n^{\text{sv}}(r_m), & i = 0, \\ p_n^{\text{dss}}(2\gamma_m, r_m, \theta_m), & i = 1, \end{cases} \quad (44)$$

where the corresponding distribution is used for $n \leq M - 1$, and the truncation bin is defined as $P(n = M|i) = 1 - \sum_{n=0}^{M-1} P(n|i)$. Here, $p_n^{\text{sv}}(r_m)$ denotes the photon number distribution of the squeezed vacuum state (Eq. (B2)), and $p_n^{\text{dss}}(\gamma_m, r_m, \theta_m)$ denotes that of the displaced squeezed vacuum state (Eq. (B4)).

The introduction of mismatch results in ζ_0 becoming a squeezed vacuum state (containing only even photon numbers), while ζ_1 becomes a displaced squeezed vacuum state whose Fock distribution generally exhibits even-odd oscillations (see Fig. 6(d)). This implies that the likelihood ratio does not necessarily vary monotonically with the photon number n . Consequently, the MAP decision generally becomes a set-based decision (potentially involving a multi-threshold structure) rather than a simple single-threshold test. Therefore, the minimum error probability (Eq. (21)) is reformulated as:

$$P_{\text{err}}^{\text{IS-K,SM}} = 1 - \frac{1}{2} \sum_{n=0}^M \max \{P(n|i=0), P(n|i=1)\}. \quad (45)$$

When employing an SPD, the observation yields only two outcomes: $n = 0$ (no-click) and $n \geq 1$ (click). Under equal priors, the MAP decision is equivalent to a binary mapping of these outcomes. Since $P(0|0) \geq P(0|1)$ (as the exponent in the latter is ≤ 0), the MAP rule maps to on-off detection: click decides symbol 1, no-click decides symbol 0. The false alarm probability is:

$$P_{\text{FA}} = P(\text{click}|0) = 1 - P(n=0|i=0) = 1 - \frac{1}{\cosh r_m}. \quad (46)$$

The miss detection probability is:

$$P_{\text{M}} = P(n=0|i=1) = \frac{1}{\cosh r_m} \exp(-|2\gamma_m|^2 + \text{Re}[e^{-i\theta_m}(2\gamma_m)^2] \tanh r_m). \quad (47)$$

These equations clearly reveal that the residual squeezing r_m reduces the vacuum component of ζ_0 , thereby increasing the false alarm probability, while θ_m modifies the vacuum overlap of ζ_1 through the exponential term.

Furthermore, we consider the saturation characteristics in the case of amplitude-only mismatch ($\Delta r \neq 0, \Delta\theta = 0$). As the signal energy tends to infinity ($N \rightarrow \infty$), the mean photon number of the signal state ζ_1 far exceeds the resolution M of the PNR detector, leading to $P_{\text{Mi}} \rightarrow 0$. In this regime, the error probability of the IS-Kennedy is dominated by the false alarm probability. The MAP strategy is thus equivalent to a threshold decision with $n_{\text{th}}^* = M$: decide symbol 1 if the detected photon number exceeds M , and symbol 0 otherwise. Since ζ_0 is a squeezed vacuum state with a non-zero photon number distribution only for even terms (see Eq. (B2)), the saturation error probability is:

$$P_{\text{sat}} \approx \frac{1}{2} P_{\text{FA}} = \frac{1}{2} \sum_{k=\lceil M/2 \rceil}^{\infty} p_{2k}^{\text{sv}}(r_m) = \frac{1}{2} \sum_{k=\lceil M/2 \rceil}^{\infty} \frac{(2k)!}{2^{2k}(k!)^2} \frac{\tanh^{2k}(r_m)}{\cosh(r_m)}. \quad (48)$$

Under the condition of small mismatch ($\Delta r \ll 1$), we have $|\Delta r| = r_m$ and $\tanh r_m \approx r_m = |\Delta r|$, and the summation is dominated by the first term. Letting $n_{\text{min}} = 2 \lceil \frac{M}{2} \rceil$, the error probability simplifies to:

$$P_{\text{sat}} \approx \frac{1}{2} p_{n_{\text{min}}}^{\text{sv}}(r_m) = \frac{1}{2} \frac{n_{\text{min}}!}{2^{n_{\text{min}}} [(n_{\text{min}}/2)!]^2} (\Delta r)^{n_{\text{min}}}. \quad (49)$$

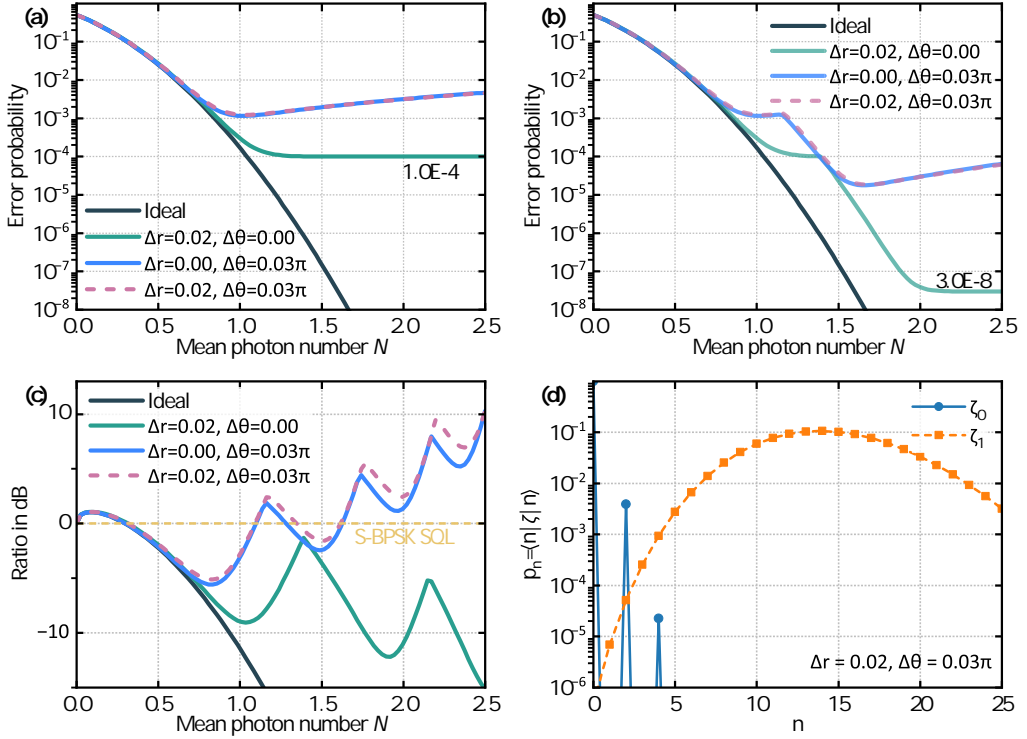


FIG. 6. Performance analysis of the IS-Kennedy receiver under inverse-squeezing mismatch conditions. (a) Error probability of IS-Kennedy with SPD. (b) Error probability of IS-Kennedy with PNR(3). (c) The performance ratio (in dB) of IS-Kennedy with PNR(10) relative to the S-BPSK SQL. (d) The Fock-basis population of ζ_0 , ζ_1 with inverse-squeezing mismatch of $\Delta r = 0.02$, $\Delta\theta = 0.03\pi$.

This equation reveals the “parity step effect” of the PNR detector in resisting mismatch: increasing the detector resolution M does not continuously reduce the saturation error probability. Instead, the order of magnitude of the error probability transitions only when M crosses an even integer threshold. Substituting $M = 1$ and $M = 3$ confirms that the calculated results are consistent with the simulation results (see Fig. 6(a) and (b)).

VI. CONCLUSION

In this paper, we proposed and analyzed an Inverse-squeezing Kennedy (IS-Kennedy) receiver for the discrimination of S-BPSK signals. By introducing an inverse-squeezing module and photon-number-resolving (PNR) detection technology, this scheme not only significantly outperforms conventional coherent-state receivers in the low-energy regime but also approaches the quantum limit (Helstrom Bound) of S-BPSK under ideal conditions. Addressing non-ideal factors in practical applications, we established a comprehensive theoretical model incorporating detection efficiency, dark counts, and squeezing mismatch. Our research reveals that the PNR detector effectively mitigates performance degradation caused by dark counts by adaptively adjusting the decision threshold. Furthermore, under squeezing mismatch conditions, a high-resolution PNR detector leverages the parity photon statistics of the squeezed vacuum state to reduce the saturation error probability by several orders of magnitude. These results demonstrate that the IS-Kennedy receiver offers a highly promising implementation scheme for high-sensitivity quantum communication based on squeezed states.

In this paper, we proposed an inverse-squeezing Kennedy (IS-Kennedy) receiver for discriminating phase-opposite displaced squeezed-vacuum states (S-BPSK). By applying a Kennedy-type nulling displacement followed by a matched inverse-squeezing operation (the inverse of the transmitter squeezing), the receiver converts the squeezing resource into an effective separation gain between hypotheses, enabling photon counting to extract the information carried jointly by displacement and squeezing. With a photon-number-resolving (PNR) detector of resolution M and a maximum a posteriori (MAP) decision rule based on the count statistics, the IS-Kennedy receiver can closely approach the S-BPSK Helstrom limit under ideal conditions and substantially outperform coherent-state baselines in the low-energy regime.

We further developed a unified performance analysis that incorporates practical imperfections, including finite detection efficiency, dark counts, finite PNR resolution, and inverse-squeezing mismatch (e.g., errors in the squeezing parameter and angle). The results reveal two key behaviors. First, in the presence of dark counts, PNR-based MAP detection improves robustness through an adaptive integer threshold, leading to characteristic step-like performance as system parameters vary. Second, inverse-squeezing mismatch introduces a parity-structured saturation (error floor) that is intrinsic to the photon-number statistics of squeezed states; importantly, increasing the PNR resolution suppresses this mismatch-induced floor in “parity steps,” with pronounced gains when the resolution crosses even-photon thresholds. Together, these findings indicate that the IS-Kennedy architecture provides a practical path toward near-optimal squeezed-state receivers using currently accessible operations—displacement, (inverse) squeezing, and photon counting.

Finally, while our model captures the dominant non-idealities for photon-counting implementations, additional experimental effects—such as displacement calibration error, local-oscillator phase noise, temporal/spectral mode mismatch, finite detector dead time, and afterpulsing—remain to be incorporated. Addressing these effects and exploring adaptive/feedback implementations constitute promising directions for future work.

Appendix A: The Wigner Function of Displaced Squeezed Vacuum States

The Displaced Squeezed States (DSSs) discussed in this paper belong to single-mode Gaussian states, whose Wigner function is a bivariate Gaussian distribution fully characterized by two parameters: the displacement vector \vec{d} and the covariance matrix \mathbf{V} . Given a DSS denoted as $|\psi\rangle$, its quantum mechanical expression is

$$|\psi\rangle = |\alpha, r\rangle = D(\alpha)S(r)|0\rangle, \quad \alpha, r \in \mathbb{R}_+. \quad (\text{A1})$$

The first parameter, the displacement vector \vec{d} , is a two-dimensional vector representing the translation in phase space relative to the origin. Its components correspond to the expectation values of the quadrature operators \hat{X}, \hat{P} :

$$\vec{d} = \begin{pmatrix} d_x \\ d_p \end{pmatrix} = \begin{pmatrix} \langle \hat{X} \rangle \\ \langle \hat{P} \rangle \end{pmatrix}. \quad (\text{A2})$$

For $|\psi\rangle$, $d_x = \sqrt{2}\operatorname{Re}(\alpha) = \sqrt{2}\alpha$ and $d_p = \sqrt{2}\operatorname{Im}(\alpha) = 0$. The second parameter, the covariance matrix \mathbf{V} , is a 2×2 real symmetric positive-definite matrix describing the “shape” and “size” of the quantum state in phase space. Its elements are variances and covariances:

$$\begin{aligned} \mathbf{V} &= \begin{bmatrix} V_{xx} & V_{xp} \\ V_{px} & V_{pp} \end{bmatrix} \\ &= \begin{bmatrix} \langle (\Delta \hat{X})^2 \rangle & \frac{1}{2} \langle \{\Delta \hat{X}, \Delta \hat{P}\} \rangle \\ \frac{1}{2} \langle \{\Delta \hat{X}, \Delta \hat{P}\} \rangle & \langle (\Delta \hat{P})^2 \rangle \end{bmatrix}, \end{aligned} \quad (\text{A3})$$

where $\Delta \hat{O} = \hat{O} - \langle \hat{O} \rangle$, and the anticommutator is defined as $\{\hat{A}, \hat{B}\} = \hat{A}\hat{B} + \hat{B}\hat{A}$. For $|\psi\rangle$, the covariance matrix is

$$\mathbf{V} = \begin{bmatrix} \frac{1}{2}e^{-2r} & 0 \\ 0 & \frac{1}{2}e^{2r} \end{bmatrix}, \quad (\text{A4})$$

indicating that in phase space, the state is an ellipse (coherent states and vacuum states appear as circles), with fluctuations squeezed along the X -direction and expanded along the P -direction, while the overall phase-space area remains unchanged ($\det \mathbf{V} = \frac{1}{2}e^{-2r} \cdot \frac{1}{2}e^{2r} = \frac{1}{4}$).

Substituting \vec{d} and \mathbf{V} into the general formula yields the Wigner function for $|\psi\rangle$:

$$\begin{aligned} W(\vec{r}|\psi) &= \frac{1}{2\pi\sqrt{\det \mathbf{V}}} \exp \left\{ -\frac{1}{2}(\vec{r} - \vec{d})^T \mathbf{V}^{-1} (\vec{r} - \vec{d}) \right\} \\ &\rightarrow W(x, p|\psi) = \frac{1}{\pi} \exp \left\{ -e^{2r} (x - \sqrt{2}\alpha)^2 - e^{-2r} p^2 \right\}, \end{aligned} \quad (\text{A5})$$

where $\vec{r} = \begin{pmatrix} x \\ p \end{pmatrix}$ is a point in phase space, and $\det \mathbf{V}$ denotes the determinant of \mathbf{V} .

Appendix B: Fock-basis Population of Squeezed Vacuum and Displaced Squeezed States

Let the Squeezed Vacuum (SV) state and the Displaced Squeezed State (DSS) be denoted, respectively, as:

$$S(z)|0\rangle \quad \text{and} \quad D(\alpha)S(z)|0\rangle, \quad (\text{B1})$$

where the squeezing parameter is complex, $z = re^{j\theta}$ (with $j = \sqrt{-1}$).

The photon number distribution of the Squeezed Vacuum (SV) state is non-zero only for even photon numbers:

$$p_{2k}^{\text{sv}}(r) = \frac{(2k)!}{2^{2k}(k!)^2} \frac{\tanh^{2k}(r)}{\cosh(r)}, \quad (\text{B2})$$

$$p_{2k+1}^{\text{sv}}(r) = 0. \quad (\text{B3})$$

The photon number distribution of the Displaced Squeezed State (DSS) can be expressed in terms of Hermite polynomials, $H_n(\cdot)$:

$$p_n^{\text{dss}} = \frac{1}{n! \cosh r} \left(\frac{\tanh r}{2} \right)^n \left| H_n \left(\frac{\alpha e^{-j\theta/2}}{\sqrt{\sinh r \cosh r}} \right) \right|^2 \exp(-|\alpha|^2 + \text{Re}[e^{-j\theta}\alpha^2] \tanh r). \quad (\text{B4})$$

ACKNOWLEDGMENTS

This work was supported by Independent Innovation Science Fund Program of National University of Defense Technology, China (Grant No. 22-ZZCX-036), Key research & development program of Guangxi (Grant No. GuiKeAB23075155), and the Key Research & Development Program of Guangxi (Grant No. AB23075112).

DATA AVAILABILITY

The data that support the findings of this article are not publicly available. The data are available from the authors upon reasonable request.

[1] R. S. Kennedy, A near-optimum receiver for the binary coherent state quantum channel, Research Laboratory of Electronics, MIT, Quarterly Progress Report **108**, 219 (1973).

[2] M. Takeoka and M. Sasaki, Discrimination of the binary coherent signal: Gaussian-operation limit and simple non-gaussian near-optimal receivers, *Phys. Rev. A* **78**, 022320 (2008).

[3] R. Yuan, M. Zhao, S. Han, and J. Cheng, Kennedy receiver using threshold detection and optimized displacement under thermal noise, *IEEE Commun. Lett.* **24**, 1313 (2020).

[4] V. A. Vilenrotter, Quantum receiver for distinguishing between binary coherent-state signals with partitioned-interval detection and constant-intensity local lasers, NASA IPN Progress Report **42** (2012).

[5] S. Izumi, M. Takeoka, M. Fujiwara, N. D. Pozza, and M. Sasaki, Quantum displacement receiver for m-ary phase-shift-keyed coherent states, *Phys. Rev. A* **86**, 042328 (2012).

[6] T. Chen, K. Li, Y. Zuo, and B. Zhu, Qam adaptive measurements feedback quantum receiver performance (2015), [arXiv:1504.02859 \[quant-ph\]](https://arxiv.org/abs/1504.02859).

[7] R. Nair, S. Guha, and S.-H. Tan, A realizable receiver for discriminating arbitrary coherent states near the quantum limit, in *2013 IEEE International Symposium on Information Theory* (2013) pp. 729–733.

[8] Y. Zuo, T. Chen, and B. Zhu, Conditional pulse nulling receiver for multi-pulse PPM and binary quantum coding signals, in *Fourth International Conference on Wireless and Optical Communications*, Vol. 9902, edited by M. Ma, International Society for Optics and Photonics (SPIE, 2016) p. 99020V.

[9] C. R. Müller, M. A. Usuga, C. Wittmann, M. Takeoka, C. Marquardt, U. L. Andersen, and G. Leuchs, Quadrature phase shift keying coherent state discrimination via a hybrid receiver, *New J. Phys.* **14**, 083009 (2012).

[10] A. Allevi, M. Bina, S. Olivares, and M. Bondani, Hybrid homodyne-like detection scheme with photon-number-resolving detectors, in *2017 Progress In Electromagnetics Research Symposium - Spring (PIERS)* (2017) pp. 2874–2878.

[11] M. N. Notarnicola, M. G. A. Paris, and S. Olivares, Hybrid near-optimum binary receiver with realistic photon-number-resolving detectors, *J. Opt. Soc. Am. B* **40**, 705 (2023).

- [12] Y. Zuo, K. Li, and B. Zhu, 16-qam quantum receiver with hybrid structure outperforming the standard quantum limit, *MATEC Web Conf.* **61**, 06008 (2016).
- [13] V. Giovannetti, S. Guha, S. Lloyd, L. Maccone, J. H. Shapiro, and H. P. Yuen, Classical capacity of the lossy bosonic channel: The exact solution, *Phys. Rev. Lett.* **92**, 027902 (2004).
- [14] M. M. Wolf, D. Pérez-García, and G. Giedke, Quantum capacities of bosonic channels, *Phys. Rev. Lett.* **98**, 130501 (2007).
- [15] L. Lami, K. K. Sabapathy, and A. Winter, All phase-space linear bosonic channels are approximately gaussian dilatable, *New J. Phys.* **20**, 113012 (2018).
- [16] C. W. Helstrom, Quantum detection and estimation theory, *J. Stat. Phys.* **1**, 231 (1969).
- [17] A. S. Holevo, Bounds for the quantity of information transmitted by a quantum communication channel, *Probl. Peredachi Inf.* **9**, 3 (1973).
- [18] M. G. A. Paris, Nearly ideal binary communication in squeezed channels, *Phys. Rev. A* **64**, 014304 (2001).
- [19] S. Izumi, M. Takeoka, K. Ema, and M. Sasaki, Quantum receivers with squeezing and photon-number-resolving detectors for m -ary coherent state discrimination, *Phys. Rev. A* **87**, 042328 (2013).
- [20] R. Schnabel, Squeezed states of light and their applications in laser interferometers, *Phys. Rep.* **684**, 1 (2017).
- [21] G. Chesi, S. Olivares, and M. G. A. Paris, Squeezing-enhanced phase-shift-keyed binary communication in noisy channels, *Phys. Rev. A* **97**, 032315 (2018).
- [22] I. A. Burenkov, M. V. Jabir, and S. V. Polyakov, Practical quantum-enhanced receivers for classical communication, *AVS Quantum Sci.* **3**, 025301 (2021).
- [23] A. Walsh, L. Conlon, B. Shajilal, O. Erkilic, J. Janousek, S. Assad, J. Zhao, and P. K. Lam, All-gaussian state discrimination beyond the coherent helstrom bound (2025), [arXiv:2510.20096 \[quant-ph\]](https://arxiv.org/abs/2510.20096).
- [24] S. M. Barnett, L. S. Phillips, and D. T. Pegg, Imperfect photodetection as projection onto mixed states, *Opt. Commun.* **158**, 45 (1998).
- [25] G. Humer, M. Peev, C. Schaeff, S. Ramelow, M. Stipčević, and R. Ursin, A simple and robust method for estimating afterpulsing in single photon detectors, *J. Lightwave Technol.* **33**, 3098 (2015).
- [26] C. Ding, X. Zhang, J. Xiong, Y. Xiao, T. Zhang, J. Huang, H. Xu, X. Liu, L. You, Z. Wang, and H. Li, Photon-number-resolving single-photon detector with a system detection efficiency of 98% and photon-number resolution of 32, *ACS Photonics* **12**, 4924 (2025).
- [27] D. Ganapathy, W. Jia, and M. Nakano (LIGO O4 Detector Collaboration), Broadband quantum enhancement of the ligo detectors with frequency-dependent squeezing, *Phys. Rev. X* **13**, 041021 (2023).
- [28] L. Gao, S. Shi, B. Lu, L.-A. Zheng, L. Tian, W. Li, Y. Wang, and Y. Zheng, Generating long-term stable squeezed states via multiple pump noise suppression, *Opt. Lett.* **50**, 4674 (2025).